

# Initial Condition of Relic Gravitational Waves Constrained by LIGO S6 and Multiple Interferometers

J.W. Chen<sup>1\*</sup>, Y. Zhang<sup>1†</sup>, W. Zhao<sup>1</sup>, M.L. Tong<sup>2</sup>

<sup>1</sup> Department of Astronomy, Key Laboratory for Researches in Galaxies and Cosmology, University of Science and Technology of China, Hefei, Anhui, 230026, China

<sup>2</sup> National Time Service Center, Chinese Academy of Sciences, Xi'an, Shaanxi 710600, China

## Abstract

The relic gravitational wave (RGW) generated during the inflation depends on the initial condition via the amplitude, the spectral index  $n_t$  and the running index  $\alpha_t$ . CMB observations so far have only constrained the tensor-scalar ratio  $r$ , but not  $n_t$  nor  $\alpha_t$ . Complementary to this, the ground-based interferometric detectors working at  $\sim 10^2$ Hz are able to constrain the spectral indices that influence the spectrum sensitively at high frequencies. In this work we give a proper normalization of the analytical spectrum at the low frequency end, yielding a modification by a factor of  $\sim 1/50$  to the previous treatment. We calculate the signal-noise ratios (SNR) for various  $(n_t, \alpha_t)$  at fixed  $r = 0.2$  by S6 of LIGO H-L. Among other things, we obtain the observational upper limit on the running index  $\alpha_t < 0.02093$  (i.e, at a detection rate 95% and a false alarm rate 5%) at  $(n_t = 0, r = 0.2)$ , as well as a loose constraint  $n_t < 0.4703$  at  $(\alpha_t = 0, r = 0.2)$ . This is consistent with the constraint on the energy density obtained by LIGO-Virgo Collaboration. Extending to the four correlated detectors currently running, the calculated SNR improves over that of LIGO H-L slightly. When extending to the second-generation, six correlated detectors in design, the calculated SNR is  $\sim 10^3$  times over the previous two cases, due to the high sensitivities. RGW can be directly detected by the six 2nd-generation detectors for models with  $\alpha_t > 0.01364$ , or  $n_t > 0.2982$ .

PACS numbers: 04.30.-w, 04.80.Nn, 98.80.Cq

## 1 Introduction

The relic gravitational wave (RGW) is believed to exist in the Universe as a stochastic background [1, 2, 3, 4, 5, 6, 7, 8, 9, 10, 11, 12, 13, 14, 15, 16, 17, 18]. The spectrum of RGW ranges over a very broad frequency band  $10^{-18} \sim 10^{10}$ Hz, and therefore serves as the scientific target of various types of gravitational detections working at different frequency bands. They includes laser interferometers ( $10^2 - 10^3$ Hz) such as LIGO [19], Virgo [20, 21], GEO [22, 23], KAGRA [24, 25, 26] and etc., and space interferometer

---

\*chjw@mail.ustc.edu.cn

†yzh@ustc.edu.cn

( $\sim 10^{-3}\text{Hz}$ ) [27, 28, 29], pulsar timing arrays ( $10^{-9} - 10^{-7}\text{Hz}$ ) [30, 31, 32, 33, 34], and CMB ( $10^{-17}\text{Hz}$ ), such as WMAP[35, 36, 37, 38, 39], Planck [40, 41], BICEP/Keck [42, 43] and etc. By 2009-2010 LIGO and Virgo data, some upper limits has been obtained on some power-law form of the energy density  $\Omega_{GW}(f)$  of the stochastic gravitational-wave background in relevant frequency bands [44].

One feature of RGW is that its amplitude is higher in lower frequency bands. The BICEP2 collaboration [43] has claimed the detection of the curl-type polarization  $C_l^{BB}$  of CMB induced by RGW around an extremely low frequency band  $f \sim 10^{-17}\text{Hz}$ . However, this signal may be mixed with the thermal radiations from galactic dust as claimed by Planck Collaboration [45]. The detection, if confirmed by other independent upcoming detections, will not be a surprise since the spectrum of RGW has the highest amplitude in this low frequency band.

After generated during the inflation, RGW is determined by its evolution during the several stages of cosmic expansion, as well as by the initial condition during inflation. For the standard Big Bang model, the analytical solution of  $h_k(\tau)$  has been obtained, covering the whole course of evolution, ranging from the inflation up to the present accelerating era [46, 47, 48, 49, 50, 51]. Within the cosmological model, the slope of the spectrum, is determined by its initial condition during the inflation, which, when the adiabatic vacuum is assumed, can be summarized into several parameters, i.e, the spectral index  $n_t$ , and the running spectral index  $\alpha_t \equiv dn_t/d\ln k$ . These two indices can be attributed to the detailed profile of the potential of the field that drives the inflation. The over amplitude of the RGW spectrum is essentially determined by the energy scale of the inflation. In this work we shall improve the choice of the overall amplitude of the spectrum, leading to a modification to our previous simple treatment [50, 51]. The amplitude can be also represented in terms of the so-called tensor-scalar ratio  $r$  when the scalar perturbation of the metric is known from other cosmological observations, such as CMB and large scale structure surveys. WMAP [38] and Planck[40], combined with BAO, SNIa, have put some constraints upon  $r$ . In particular, BICEP2 has given  $r = 0.2$  under the default  $n_t = 0$ . However, since the observational data of  $C_l^{BB}$  is within  $l = (50 \sim 150)$ , corresponding to a very narrow band, the observational result puts little constraints on the indices  $n_t$  and  $\alpha_t$ .

Nevertheless, interferometers like LIGO and etc, combined with the results of CMB, can put effective constraints on  $n_t$ , and especially on  $\alpha_t$ . This is because the profile of the RGW spectrum is very sensitive to  $n_t$  and  $\alpha_t$  at high frequencies, i.e, ( $10^2 - 10^3$ )Hz at which LIGO and Virgo are working. Therefore, with regard to detections of RGW, the laser interferometers and the observation of  $C^{BB}$  of CMB are complementary. In our previous work [51], the LIGO S5 data [52] were used to constrain  $n_t$  and  $\alpha_t$ , assuming an over-estimated ratio  $r = 0.55$ . Now with the improved LIGO S6 data[53] and  $r = 0.2$  of BICEP2, we shall use the analytical spectrum of RGW to calculate SNR with the correlation between LIGO H1 and L1, obtain an upper limits of  $\alpha_t$  and  $n_t$ .

Correlating more detectors will provide more accurate measurements. By correlating the four 1st-generation detectors, i.e, LIGO-Hanford, LIGO-Livingston, Virgo and GEO, using the data of sensitivity from their scientific runs, we calculate the optimal SNR and arrive at the detection limits of  $\alpha_t$  and  $n_t$ , whereby two different methods are adopted: multiple pairs and four-detector correlation. The 2nd-generation detectors are under construction, such as the advanced LIGO [54] and the advanced Virgo, and KAGRA [24], AIGO [55], LIGO-India [56, 57]. Their sensitivities of design will reach  $\sim 10^{-23}$ . We also extend the calculation to the 2nd-generation detectors by correlating six ones.

In section 2, we examine the properties of the spectrum of RGW that are determined

by the initial condition during the inflation, and give a modification of its initial amplitude under the quantum normalization.

In section 3, we calculate SNR for various values of  $\alpha_t$  and  $n_t$ , and obtain an upper limit on  $\alpha_t$ , based on the data of LIGO S6 and the CMB observations.

In section 4, the calculations are extended to the four detectors in operation, in two ways of combinations: (1) multiple pairs, and (2) four-detector correlation.

In section 5, we extend to the six detectors of 2nd-generation under construction.

In Appendix, we write down the formula of the overlapping function used in calculating SNR of the pairs of detectors, and list the information of positions and orientations of seven detectors involved.

## 2 Analytical spectrum of RGW: Normalization of Amplitude

Consider a spatially flat RW spacetime,

$$ds^2 = a^2(\tau)[d\tau^2 - (\delta_{ij} + h_{ij})dx^i dx^j], \quad (1)$$

where  $\tau$  is the conformal time, and the perturbations  $h_{ij}$  denotes RGW in the traceless and transverse gauge, and can be written in terms of its Fourier and polarization modes

$$h_{ij}(\mathbf{x}, \tau) = \frac{1}{(2\pi)^{3/2}} \int d^3k e^{i\mathbf{k}\cdot\mathbf{x}} \sum_{s=+,\times} \overset{s}{\epsilon}_{ij}(k) \overset{s}{h}_k(\tau), \quad \mathbf{k} = k\hat{k}, \quad (2)$$

with two polarization tensors satisfying

$$\overset{s}{\epsilon}_{ij}(k)\delta_{ij} = 0, \quad \overset{s}{\epsilon}_{ij}(k)k^i = 0, \quad \overset{s}{\epsilon}_{ij}(k)\overset{s'}{\epsilon}_{ij}(k) = 2\delta_{ss'}.$$

The polarizations modes  $+, \times$  are assumed to be statistically equivalent. In this case the superscript  $s$  can be dropped, the evolution of the Fourier mode  $h_k(\tau)$  of RGWs is

$$h_k''(\tau) + 2\frac{a'(\tau)}{a(\tau)}h_k'(\tau) + k^2h_k(\tau) = 0, \quad (3)$$

where  $k$  is the conformal wavenumber. For each stage of of the Big-Bang expansion, i.e, inflation, reheating, radiation dominant, matter dominant and dark energy dominant, the scale factor is of a generic form  $a(\tau) \propto \tau^d$  and  $a'/a = d/\tau$ , the solution of Eq.(3) is simply a combination of two Bessel functions,  $\tau^{d-1/2}J_{d-1/2}$  and  $\tau^{d-1/2}J_{-d+1/2}$ . As a prominent property of RGW, for any stage, the solution of Eq.(3) approaches to a constant,  $h_k(\tau) \sim \text{const}$  for  $k \ll a'/a$ , and takes approximately a form  $h_k(\tau) \sim e^{ik\tau}/a(\tau)$  for  $k \gg a'/a$ , i.e, the long-wavelength modes remain constant, whereas the short-wavelength mode decrease as  $1/a(\tau)$  with the cosmic expansion. By joining these stages, the full analytical solution  $h_k(\tau)$  has been obtained, which covers the whole course of evolution [46, 47]. Some processes occurred during the cosmic expansion, such as neutrino free-streaming [48],  $e^+e^-$  annihilation and QCD transition [49], can cause small suppressions of the amplitude of RGW. We shall not include these minor effects in this paper. The initial condition of  $h_k(\tau)$  during the inflation will be fixed either by theoretical considerations or by actual observations. Most of literature of RGW are about its generation during inflation and the transition to RD stage, and few cover the five stages mentioned above.

The RGW spectrum is defined by

$$\int_0^\infty h^2(k, \tau) \frac{dk}{k} \equiv \langle 0|h^{ij}(\mathbf{x}, \tau)h_{ij}(\mathbf{x}, \tau)|0\rangle, \quad (4)$$

where  $\langle 0|\dots|0\rangle$  denotes the expectation value. Substituting Eq.(2) into Eq.(4) leads to the spectrum in terms of the mode  $h_k(\tau)$ :

$$h(k, \tau) = 4\sqrt{\pi}k^{3/2}|h_k(\tau)|. \quad (5)$$

When  $\tau$  is set to be the present time  $\tau_H$ , it gives the present spectrum, and when  $\tau$  is set to be the ending time  $\tau_1$  of the inflation, it will give the primordial spectrum.

To fix the mode  $h_k(\tau)$  completely, the initial condition has to be specified during the inflation, for which the scale factor  $a(\tau) = H^{-1}|\tau|^{1+\beta}$  with  $\beta \simeq -2$  and  $H$  being the inflation rate. We like to emphasize that the model here is quite general, and includes a large class of inflation models as long as  $a(\tau) \propto |\tau|^{1+\beta}$ . It does not necessarily rely on some scalar inflaton. The solution for the inflationary stage is

$$h_k(\tau) = A_k H k^{1+\beta} |x|^{-(\frac{1}{2}+\beta)} [A_1 J_{\frac{1}{2}+\beta}(x) + A_2 J_{-(\frac{1}{2}+\beta)}(x)], \quad (6)$$

where  $x \equiv k\tau$ , two coefficients  $A_1 = \frac{-i}{\cos \beta \pi} \sqrt{\frac{\pi}{2}} e^{i\pi\beta/2}$  and  $A_2 = iA_1 e^{-i\pi\beta}$  are taken so that  $h_k(\tau) \propto H_{\frac{1}{2}+\beta}^{(2)}(k\tau)$  and  $\lim_{k \rightarrow \infty} h_k(\tau) \propto e^{-ik\tau}$ . This choice of the initial state is also called the adiabatic vacuum [58]. The coefficient factor  $A_k = \frac{\sqrt{G}}{\pi\sqrt{k}}$  is the initial amplitude determined by the so-called quantum normalization [59, 60], i.e, each  $\mathbf{k}$ -mode in the initial vacuum has a zero point energy  $\frac{1}{2}\hbar(\frac{2\pi k}{a})$  where  $\hbar$  is the Planck constant. In the long wavelength limit, the primordial spectrum takes the following power-law form

$$h(k, \tau_1) = A \left(\frac{k}{k_0}\right)^{2+\beta} + O(k), \quad (7)$$

where  $A \simeq \frac{\sqrt{2}}{\pi} \frac{H}{M_{Pl}}$  and  $M_{Pl}$  is the Planck mass, and  $k_0$  is a pivot conformal wavenumber often used in CMB observations, corresponding to a physical wavenumber  $k_0/a(\tau_H) = 0.002 Mpc^{-1}$ . In literature [36], the leading portion of the primordial spectrum (7) is often rewritten as

$$\Delta_h(k) = \Delta_R r^{1/2} \left(\frac{k}{k_0}\right)^{\frac{n_t}{2} + \frac{1}{4}\alpha_t \ln(\frac{k}{k_0})}, \quad (8)$$

where  $r \equiv \Delta_h^2(k_0)/\Delta_R^2(k_0)$  is the tensor-scalar ratio, the tensorial spectral index  $n_t = 2\beta + 4 \equiv d \ln \Delta_h^2/d \ln k|_{k=k_0}$ , and  $\alpha_t \equiv d^2 \ln \Delta_h^2/d \ln k^2|_{k=k_0}$  is the spectral running index also introduced, allowing for variations from the power-law spectrum in Eq.(7). Higher running indices can be further introduced [61], but we are still restricted to only  $n_t$  and  $\alpha_t$  in this paper, as only few observational data are available currently. Although  $n_t$  and  $\alpha_t$  are formally the coefficients of Taylor series in terms of  $\ln(k/k_0)$ , this does not necessarily mean that  $\alpha_t$  would be subdominant to  $n_t$  in affecting the spectrum. In the frequency range around  $f \sim 10^2 \text{Hz}$  for LIGO concerned in here, the height of the spectral amplitude of RGW is more sensitive to the value of  $\alpha_t$  than  $n_t$ , comparatively, as Fig.3 and Fig.4 demonstrate. In our model of RGW,  $r$ ,  $n_t$  and  $\alpha_t$  by definition in (8) are three independent parameters describing the primordial spectrum. Theoretically, they are predicted by the detail of the specific inflation models. For instance,  $r$  is proportional to  $V$ ,  $n_t$  is a function of  $V'$  (the slope of the potential), and  $\alpha_t$  is a function of  $V'$  and  $V''$  (the curvature of the potential) in scalar inflation models [61]. For generic inflation models, these three parameters can be independent. Although there have been observational results and constraints on the spectral index and running spectral index of the scalar perturbations, so far, there is no direct observation on  $r$ ,  $n_t$  and  $\alpha_t$  of RGW beside BICEP2. Some very weak constraints on  $r$  have only been given by CMB observations [37, 38, 39, 41], and this might further infer a constraint on  $n_t$  via the consistency relation within the scalar

inflation models, and different models will give different relations such as  $n_t = -r/8$ , and its variants, etc, [62, 63, 64, 65, 66]. Most inflation modes predict the value of  $n_t$  to be around 0. So, in absence of an observed value of  $n_t$  and  $\alpha_t$ , we shall take various values of  $n_t$  around 0 in constraining  $\alpha_t$ , and vice versa, in this paper.

Fig.1 shows the primordial spectrum  $h(k, \tau_1)$  with  $n_t = \alpha_t = 0$  as the top curve, and also other two representative curves of  $h(k, \tau)$  at the redshift  $z = 1100$  and at present, respectively. Fig.1 tells the pattern of the evolution of  $h(k, \tau)$ , which is decreasing with time in high frequencies. In the expression (8),  $\Delta_R$  is the curvature perturbation at  $k_0$ , which is, by WMAP9+eCMB+BAO+ $H_0$  observations [39],

$$\Delta_R^2 = (2.464 \pm 0.072) \times 10^{-9}, \quad (9)$$

and the tensor-scalar ratio  $r < 0.13$  (95%CL). Note that the constraint  $r < 0.11$  (95%CL) with no scalar running, and  $r < 0.26$  (95%CL) including scalar running, are given by Planck measurement [41]. BICEP2 [43] gives

$$r = 0.20_{-0.05}^{+0.07}, \quad (10)$$

under the condition  $n_t = 0$  independent of the pivot scale. The consistency relation would give  $n_t > -0.016$  by WMAP9 [39]. If we were to use the consistency relation, the BICEP2 would give  $n_t = -0.025$ . An likelihood analysis is made on the parameters  $(r, n_t)$  [67], viewing that only with WMAP+Planck one cannot impose any constraint on  $n_t$  using the value of  $r$ . Ref. [67] uses the probability distribution of  $r$  as the prior obtained from BICEP2 [43], in combination of the likelihood contour of  $(r, n_t)$  from the WMAP+Planck data, arrive at a probability distribution of  $n_t$ , scattering around a value  $n_t \sim 0.1$  loosely, which is a poor constraint on  $n_t$ . Facing this situation of absence of an observed value  $n_t$ , we take  $(n_t = \alpha_t = 0, r = 0.20)$  as the default values of RGW, since our model in this paper of the initial condition of RGW is generic, which can correspond to a large class of inflation models. We shall compute SNR of RGW for various values of  $(n_t, \alpha_t, r)$ .

As mentioned earlier, those modes  $h_k(\tau)$  remain constant if  $k \ll a'/a$  during the whole course of evolution. Therefore, the low frequency end of the present spectrum will remain the same as that of the primordial spectrum, as shown in Fig.1,

$$h(k, \tau_H) = h(k, \tau_1) \quad \text{for} \quad \frac{k}{2\pi a(\tau_H)} \ll H_0, \quad (11)$$

where  $H_0 = 3.24h \times 10^{-18}\text{Hz}$  is the present Hubble constant with  $h \simeq 0.69$  [38]. This will tell us how to fix the undetermined amplitude of  $h(k, \tau_H)$ . We first plot the primordial  $h(k, \tau_1)$  according to Eq.(8), which is a roughly flat curve as shown in Fig. 2. Then, we take the low-frequency end of the present spectrum  $h(k, \tau_H)$  of Eq.(5) to be overlapping with that of the given  $h(k, \tau_1)$ . This fixes the overall amplitude of  $h(k, \tau_H)$ . In our previous treatment [50, 51], the amplitude at a frequency of the horizon-cross ( $f \simeq H_0$ ) was taken to be equal to the primordial value  $h(k, \tau_1)$  at the same  $f$ . This would lead to an overestimated amplitude (dashed line), as Fig. 2 shows. Our present paper corrects it by the proper normalization, reducing by a factor  $\sim 50$ .

The resulting spectrum  $h(f, \tau_H)$ , drawn in Fig.3 and Fig.4 for various  $n_t$  and  $\alpha_t$ , shows the prominent feature that it is high at low frequencies and low at high frequencies. At the low frequencies ( $10^{-18} - 10^{-15}\text{Hz}$ ),  $h(f, \tau_H) \sim (10^{-6} - 10^{-9})$  induces CMB anisotropy and polarization at large angles  $l = (2 \sim 2000)$  [68, 69, 70, 71]. In particular,  $C_l^{BB}$  detected by BICEP2 [43] around  $l = 50 \sim 150$  is induced by  $h(f, \tau_H) \sim (10^{-9} \sim 10^{-8})$  in a band ( $5 \times 10^{-18} \sim 5 \times 10^{-17}\text{Hz}$ ). At the median frequencies ( $10^{-9} - 10^{-7}\text{Hz}$ ,

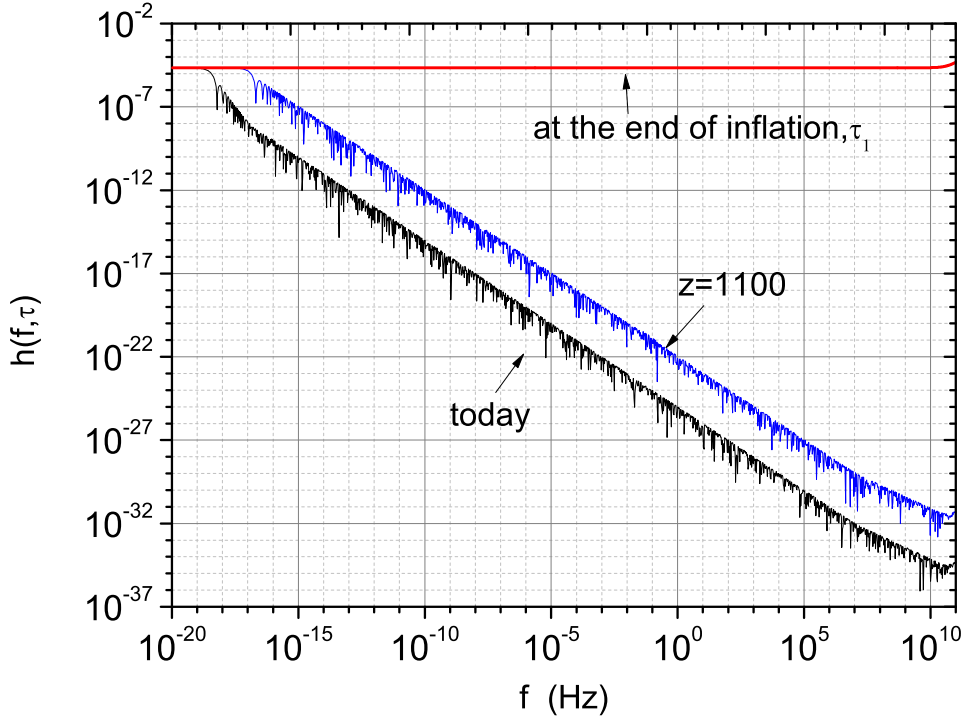


Figure 1: The evolution of RGW spectrum at the fixed parameter  $n_t = 0$  and  $\alpha_t = 0$ . The horizontal axis is the present physical frequency  $f = \frac{k}{2\pi a(\tau_H)}$ .

$h(f, \tau_H) \sim (10^{-17} - 10^{-16})$  can be the target of PTA [60]. In this paper we are mainly concerned with the high frequency band ( $10^2 - 10^3$ )Hz for interferometers where  $h(f, \tau_H) \sim (10^{-26} \sim 10^{-27})$ . The very high frequency band around  $\sim 10^9$ Hz can be the target of the detectors using a polarized maser [72]. But for  $f \geq 10^{10}$ Hz, the spectrum should be subject to a regularization to subtract the divergent part of the vacuum [73, 74, 75], an issue not to be addressed here.

A very important property of  $h(f, \tau_H)$  is that its high frequency portion depends sensitively on the indices  $n_t$  and  $\alpha_t$ . A small variation of  $n_t$  and  $\alpha_t$  will cause a considerable change of the amplitude at high frequencies. In particular, at  $10^2 \sim 10^3$ Hz at which interferometers are working, an increase of  $\alpha_t$  by 0.01 causes an increase of amplitude  $h(f, \tau_H)$  by more than two to three orders of magnitude. It is this property that LIGO currently running can constrain stringently  $\alpha_t$ , and less stringently on  $n_t$  comparatively, as we shall demonstrate in the following.

The energy density of RGW is  $\Omega_g = \rho_g / \rho_c$ , where  $\rho_g = \frac{1}{32\pi G a^2} h'_{ij} h'^{ij}$  and  $\rho_c = 3H_0^2 / 8\pi G$ . The spectral energy density  $\Omega_g(f)$  is defined by  $\Omega_g = \int \Omega_g(f) df / f$ , and in terms of  $h(f, \tau_H)$ , the spectral energy density is given by

$$\Omega_g(f) = \frac{\pi^2}{3} h^2(f, \tau_H) \left(\frac{f}{H_0}\right)^2, \quad (12)$$

depending on the parameters  $n_t$ ,  $\alpha_t$  and  $r$  via  $h(f, \tau_H)$ . It will be used later in Eq.(16) in calculating SNR for a pair of two detectors. As shown in Fig.5, for the default ( $n_t = \alpha_t = 0, r = 0.20$ ),  $\Omega_g(f)$  is rather flat with a height  $\sim 10^{-14}$  within a large portion of frequency range.

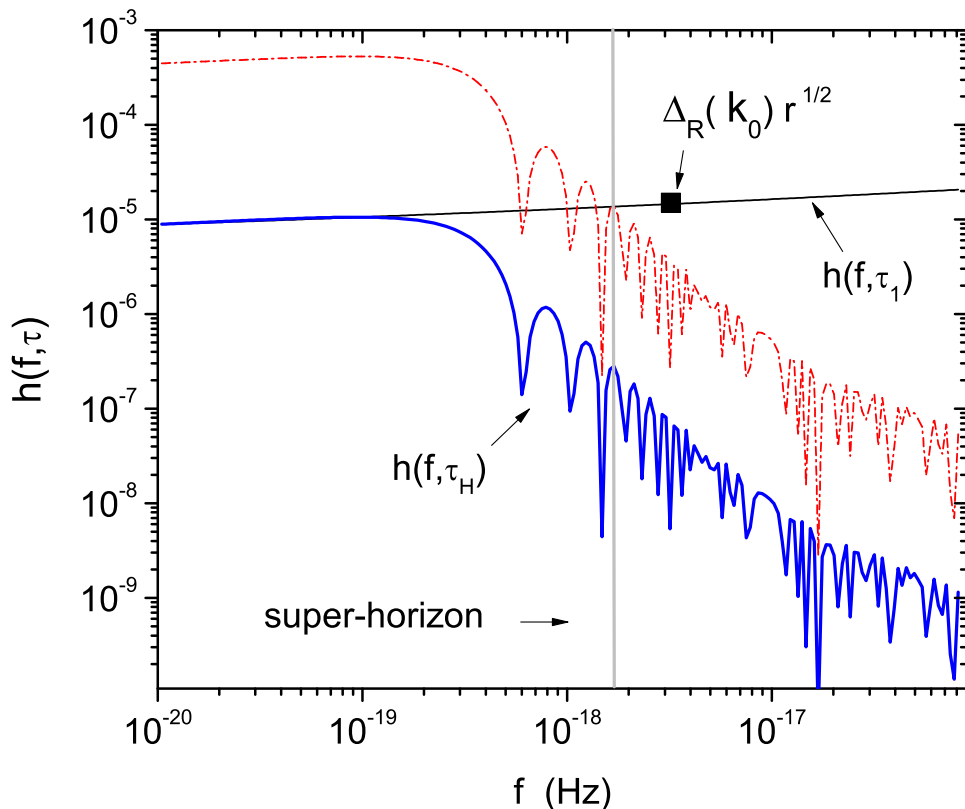


Figure 2: The choice of the amplitude of the present spectrum of RGW. Here  $r = 0.20$ ,  $n_t = 0.2$ ,  $\alpha_t = 0.01$  are taken for demonstration. The above dashed curve is the overestimated spectrum in our previous work.

### 3 Constraint by LIGO S6

#### 3.1 Constraint by a Single Detector of LIGO S6

First let us estimate the constraints on RGW by a single LIGO S6 detector running from 2009 July 7 to 2010 Oct 20 [53]. The previous work [51] did for LIGO S5, which was less sensitive than S6. For RGW to be detectable by a single detector of a strain sensitivity  $\tilde{h}_f$ , the simple condition is

$$h_c(f)\sqrt{F/2f} \geq \tilde{h}_f, \quad (13)$$

where  $h_c(f) = h(f, \tau_H)/\sqrt{2}$  is the characteristic amplitude of RGW,  $\tilde{h}_f$  is the amplitude of noise of the detector, which is given in Ref.[53] for S6 H1 and L1 (of 2010-05), and  $F = 2/5$  is the angular factor. Although RGW has not been detected by LIGO S6, RGW is already constrained, using Eq.(13). We plot  $h_c(f)\sqrt{F/2f}$  so that it is not greater than  $\tilde{h}_f$ . This is carried out for various values of  $n_t$  and  $\alpha_t$  at  $r = 0.2$ , and two specific combinations are shown in Fig. 6. For a comparison,  $\tilde{h}_f$  of S5 [52] is also added into the plot. Obviously S6 has a lower  $\tilde{h}_f$  than that of S5, yielding a more stringent constraints upon RGW. The resulting constraint by a single detector of LIGO S6 the resulting constraint on the index is

$$n_t < 0.612 \quad (14)$$

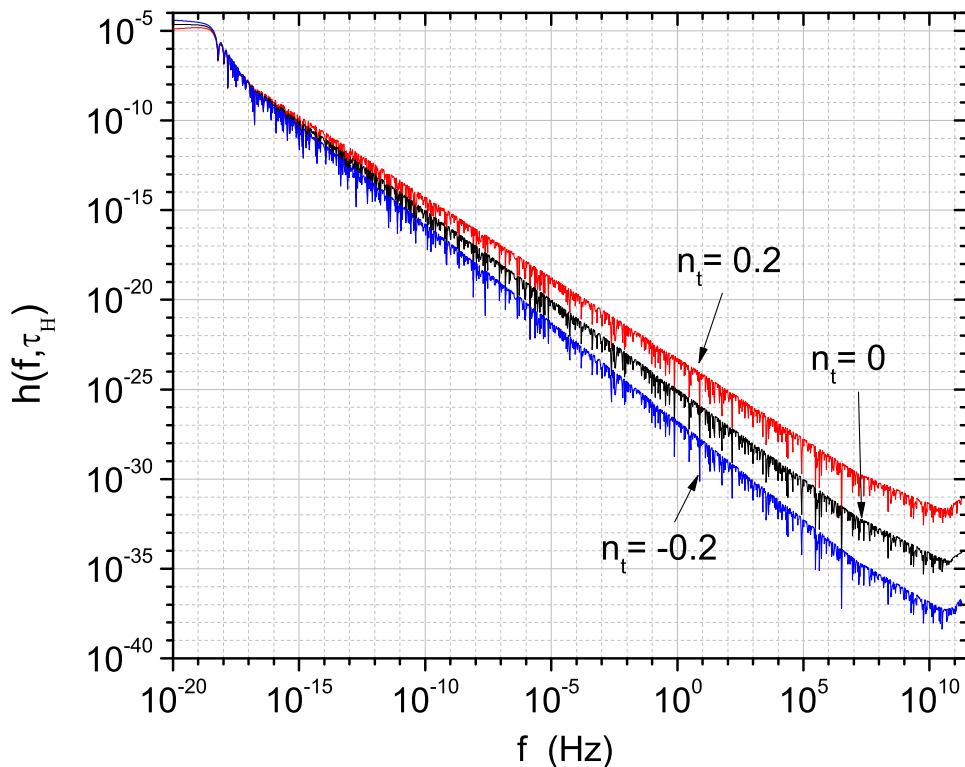


Figure 3: The RGW spectrum for various  $n_t$  at  $\alpha_t = 0$ ,  $r = 0.2$ .

at  $\alpha_t = 0$  and  $r = 0.2$ , and on the running index is

$$\alpha_t < 0.0272 \quad (15)$$

at the default  $r = 0.2$  and  $n_t = 0$ . The constraint on  $n_t$  is not as stringent as that on  $\alpha_t$ . This is because the amplitude  $h(f, \tau_H)$  around  $(10^2 - 10^3)$ Hz depends less sensitively to  $n_t$  than to  $\alpha_t$ , **as mentioned earlier**.

### 3.2 Constraint by the pair of LIGO S6

In order to be able to detect gravitational waves, one needs at least two correlated detectors. Correlating two or more interferometers will increase the capability to detect RGW and to strengthen the constraint on  $\alpha_t$ . We consider the two interferometers, LIGO H1 and L1 that have been successfully running as designed, and calculate the SNR using the S6 data of the pair [53]. In the following, we simply denote H for H1 and L for L1.

For any two interferometer detectors  $i$  and  $j$ , the formula of SNR is given by [76, 77]:

$$\text{SNR}_{ij} = \frac{3H_0^2}{10\pi^2} \sqrt{T} \left[ \int_{-\infty}^{\infty} df \frac{\gamma^2(f) \Omega_g^2(f)}{f^6 P_i(f) P_j(f)} \right]^{1/2}, \quad (16)$$

where  $H_0$  is the Hubble constant,  $\Omega_g(f)$  is given in Eq.(12) from our calculation, depending on  $(n_t, \alpha_t, r)$ , and  $P_i(f) = |\tilde{h}_f|^2$  is the power spectral density of the noise of the detector  $i$ . For S6, we take  $\tilde{h}_f$  from Ref.[53].  $T$  is the duration of detection, 1.282 years for LIGO S6.  $\gamma(f)$  is the overlap reduction function between two detectors, depending on their positions and directions. Our calculation of  $\gamma(f)$  is attached in Appendix for the relevant pairs of seven detectors considered in this paper.



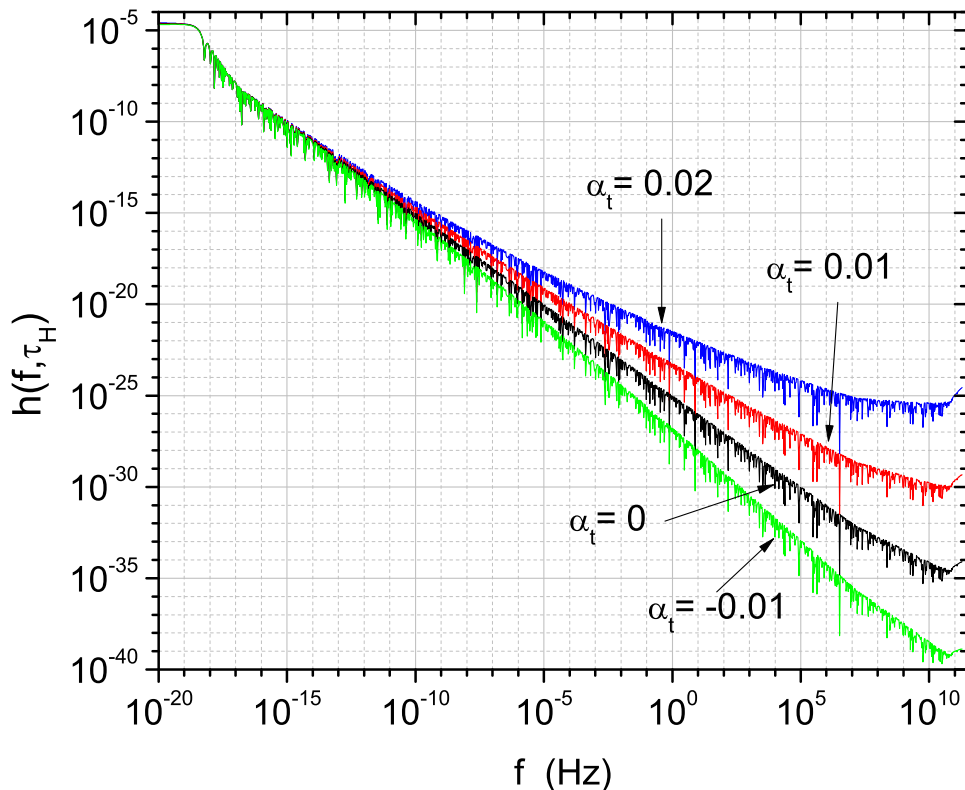


Figure 4: The RGW spectrum for various  $\alpha_t$  at  $n_t = 0$ ,  $r = 0.2$ .

Table 1 shows our integration result of SNR for S6 of LIGO H-L. For comparison, we also calculate for S5 [52]. It is seen that the detection capability of S6 improves over that of S5. We mention that in our previous work [51], an overestimated amplitude of RGW was used.

Table 1:  $\text{SNR}_{\text{HL}}$  for various  $\alpha_t, n_t$  at  $r = 0.2$ . LIGO S5 is also listed for a comparison.

$\alpha_t, n_t$	-0.005, -0.1	0, 0	0.005, 0.1	0.01, 0.2	0.015, 0.2
S5	$1.6 \times 10^{-13}$	$1.9 \times 10^{-9}$	$2.3 \times 10^{-5}$	$3.0 \times 10^{-1}$	$4.4 \times 10^1$
S6	$1.6 \times 10^{-13}$	$2.2 \times 10^{-9}$	$3.1 \times 10^{-5}$	$4.2 \times 10^{-1}$	$6.6 \times 10^1$

A constraint on  $\alpha_t$  can be also given from these data of the LIGO pair. Since SNR is implicitly a function of  $\alpha_t$  via the integrand  $\Omega_g(f)$  at fixed  $n_t$  and  $r$ . Given a value of SNR, a corresponding  $\alpha_t$  will follow from Eq.(16). In fact, in the Frequentist approach of statistic, SNR depends on the false alarm rate  $\alpha$  and the detection rate  $\gamma$  that we require for a detection. Explicitly, the relation is (Eq.(4.36) of [77]):

$$\text{SNR}_{\alpha, \gamma}^2 = 2 \left( \text{erfc}^{-1}(2\gamma) - \text{erfc}^{-1}(2\alpha) \right)^2, \quad (17)$$

where  $\text{erfc}^{-1}$  is the inverse complementary error function. This relation of Eq.(17) holds regardless of RGW. On the other hand, if the calculated SNR of RGW by Eq.(16) is greater than  $\text{SNR}_{\alpha, \gamma}$ , the RGW signal can be effectively detected at the rates  $\alpha$  and  $\gamma$  as we require. Let us take  $\alpha = 0.05$  and  $\gamma = 0.95$  for example. Then Eq.(17) yields a value

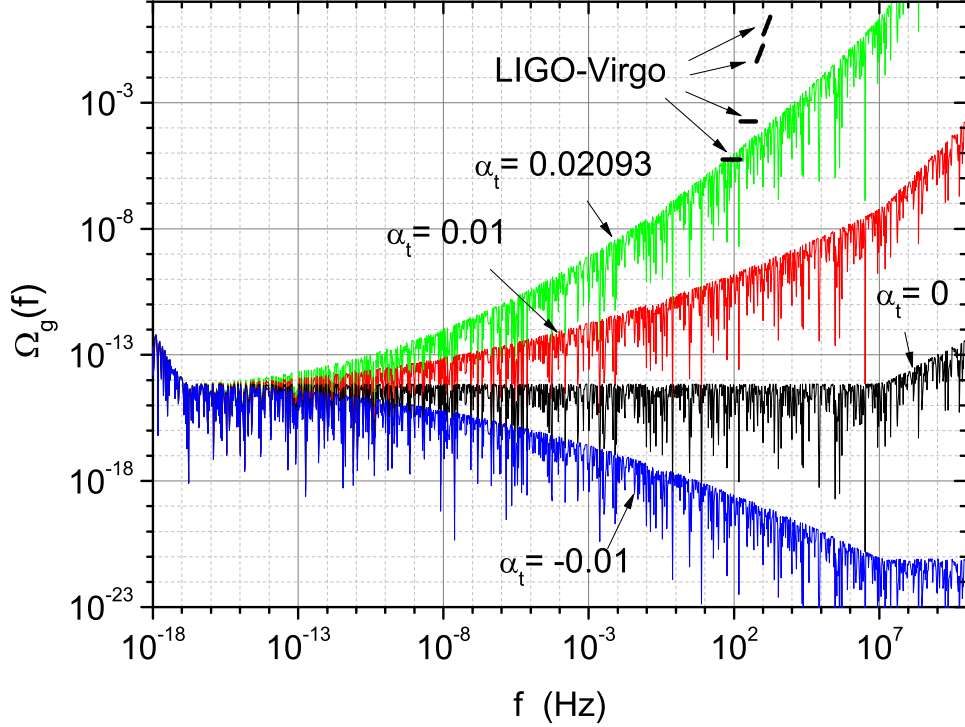


Figure 5: The spectrum of energy density for various  $\alpha_t$  at  $r = 0.2$ ,  $n_t = 0$ . LIGO-Virgo data are from Ref [44].

$\text{SNR}_{\alpha,\gamma} = 3.30$ . Since RGW has not yet detected by LIGO S6, the calculated SNR of RGW is then less than 3.30.

Thereby, a constraint on  $n_t$  can be given at fixed  $\alpha_t$  and  $r$ . The result is shown in Table 2. Inflation models not satisfying the constraints will be ruled out. In particular, at  $\alpha_t = 0$  and  $r=0.2$ , S6 of LIGO pair on the index is

$$n_t < 0.4703, \quad (18)$$

which is a loose but direct constraint, consistent with those from CMB observations, listed below Eq.(10). Similarly, a constraint on  $\alpha_t$  can be given at fixed  $n_t$  and  $r$ . shown in Table 3 and Fig.7. And at  $n_t = 0$  and  $r=0.2$ , the constraint of S6 of LIGO pair on the running index is

$$\alpha_t < 0.02093, \quad (19)$$

more stringent than that in Eq.(15) of a single detector. Table 3 is the first constraint on the running index  $\alpha_t$  based on actual observations. The observations of CMB so far have no constraint on  $\alpha_t$  because the large angular data of CMB are not very sensitive to  $\alpha_t$ . This also shows the advantage of interferometers as a complementary to those CMB observations.

We notice that LIGO and Virgo [44] use the data of 2009-2010 and give the constraints on the total energy density of a general stochastic gravitational-wave background, at four different frequency bands. These are also plotted in Fig. 5 to compare with our constraints. As Fig. 5 shows clearly, in particular, their constraint  $\Omega_{GW}(f) < 5.6 \times 10^{-6}$  in (41 – 169)Hz is consistent with our constraint in Eq.(19). However, the other three upper limits of theirs are quite higher than our  $\Omega_g(f)$  for the case  $\alpha_t = 0.02093$ . It is remarked that the constraints on the specific parameters of RGW have been made possible with the help of the analytical solution of RGW.

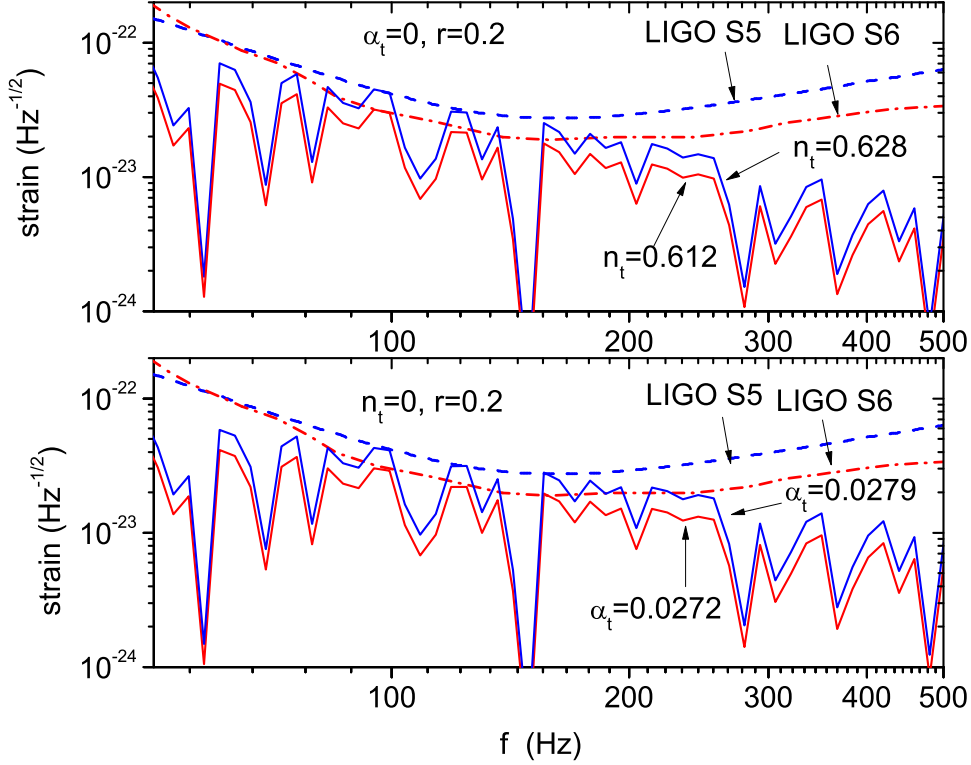


Figure 6:  $h_c(f)\sqrt{F/2f}$  vs  $\tilde{h}_f$ . This leads to constraints on RGW by a single detector of LIGO. Top: upper limits of  $n_t$  at  $\alpha_t = 0$  and  $r = 0.2$ ; Bottom: upper limits of  $\alpha_t$  at  $n_t = 0$  and  $r = 0.2$ .

## 4 Detection by four detectors of 1st-generation

More detectors correlated have a higher capability to directly detect RGWs. Now we calculate the SNRs of four correlated detectors: LIGO-Hanford(H), LIGO-Livingston(L) and Virgo(V), Geo(G). These detectors have carried out the scientific runs, and their data of sensitivities  $|\tilde{h}_f|$  are available. For H and L, we use LIGO S6 data; and for V, we use the VSR2 data. These three sets data are reported in Fig.1 of reference [53]. For Geo, we use the Geo600 sensitivity [22]. Although these four detectors actually run at different time and over different durations, for simplicity of our calculation, we suppose they were running at the same time and for the same duration  $T = 1.282$  years as LIGO S6. There are two ways to combine 4 detectors to sum up the total of the optimal SNR [77]: (1) multiple pairs; (2) four-detector correlation.

### 4.1 multiple pairs

Four detectors can be grouped into 6 pairs, each pair consists of 2 correlated detectors, and there is no correlation between different pairs. For the four detectors of G, H, L and V, the squared optimal SNR of multiple pairs is (Eq.(5.46) in Ref.[77])

$$\text{SNR}_{\text{optimal}}^2 = \text{SNR}_{\text{GH}}^2 + \text{SNR}_{\text{GL}}^2 + \text{SNR}_{\text{GV}}^2 + \text{SNR}_{\text{HL}}^2 + \text{SNR}_{\text{HV}}^2 + \text{SNR}_{\text{LV}}^2, \quad (20)$$

where  $\text{SNR}_{ij}^2$  of each pair on the right hand side will be calculated by the formula in Eq.(16). Eq.(20) indicates that  $\text{SNR}_{\text{optimal}}^2$  of multiple pairs is always greater than the  $\text{SNR}_{ij}^2$  of any pair. Using the overlapping function  $\gamma(f)$  and the relevant information of the positions and orientations in Appendix, we calculate each  $\text{SNR}_{ij}^2$  involved in Eq.(20),

Table 2: The upper limits of  $n_t$  constrained by the pair of LIGO S6, at the false alarm rate  $\alpha = 5\%$  and the detection rate  $\gamma = 95\%$ .

	$\alpha_t = -0.01$	$\alpha_t = 0$	$\alpha_t = 0.01$	$\alpha_t = 0.02$	$\alpha_t = 0.03$
$r = 0.1$	0.7103	0.4858	0.2613	0.0363	-0.1886
$r = 0.15$	0.7012	0.4769	0.2522	0.0273	-0.1976
$r = 0.2$	0.6949	0.4703	0.2457	0.0209	-0.2039
$r = 0.25$	0.6899	0.4653	0.2407	0.0160	-0.2089
$r = 0.3$	0.6858	0.4612	0.2367	0.0120	-0.2129

Table 3: The upper limits of  $\alpha_t$  constrained by the pair of LIGO S6, at the false alarm rate  $\alpha = 5\%$  and the detection rate  $\gamma = 95\%$ .

	$n_t = -0.2$	$n_t = -0.1$	$n_t = 0$	$n_t = 0.1$	$n_t = 0.2$
$r = 0.1$	0.03051	0.02606	0.02162	0.01717	0.01272
$r = 0.15$	0.03011	0.02566	0.02122	0.01677	0.01232
$r = 0.2$	0.02982	0.02538	0.02093	0.01648	0.01203
$r = 0.25$	0.02960	0.02516	0.02071	0.01626	0.01181
$r = 0.3$	0.02942	0.02478	0.02053	0.01608	0.01173

yielding  $\text{SNR}_{\text{optimal}}^2$ . The result is shown in Table 4. It is seen that  $\text{SNR}_{\text{optimal}}^2$  is greater than  $\text{SNR}_{\text{HL}}$  for the LIGO H-L pair in Table 1 by only about 10%  $\sim$  20%. This is because the main contribution to  $\text{SNR}_{\text{optimal}}^2$  is from LIGO H-L pair, which has the highest sensitivities.

Table 4:  $\text{SNR}_{\text{optimal}}$  of the multiple pairs from four detectors at  $r = 0.2$ .

$\alpha_t, n_t$	-0.005, -0.1	0, 0	0.005, 0.1	0.01, 0.2	0.015, 0.2
SNR	$1.9 \times 10^{-13}$	$2.6 \times 10^{-9}$	$3.5 \times 10^{-5}$	$4.8 \times 10^{-1}$	$7.5 \times 10^1$

Similar to the last section, by requiring  $\text{SNR}_{\text{optimal}} > \text{SNR}_{\alpha, \gamma} = 3.30$ , the multiple pair can directly detect RGW for certain value of  $\alpha_t$ , as shown in Table 5. The minimum  $\alpha_t$  required to be detected by 4 detectors is lower than the constraint of LIGO pair S6, comparing to Table 3. In particular, for  $n_t = 0$  and  $r = 0.2$ , the minimum  $\alpha_t = 0.02080$  for the multiple pairs is smaller than the constraint  $\alpha_t < 0.02093$  for S6 of LIGO pair.

## 4.2 four-detector correlation

Four detectors can also be treated as a group of 4 correlated detectors, the corresponding squared optimal SNR is (Eq.(5.91) in [77])

$$\text{SNR}_{\text{optimal}}^2 = \text{SNR}_{\text{GH}}^2 \text{SNR}_{\text{LV}}^2 + \text{SNR}_{\text{GL}}^2 \text{SNR}_{\text{HV}}^2 + \text{SNR}_{\text{GV}}^2 \text{SNR}_{\text{HL}}^2. \quad (21)$$

In this case, the optimal  $\text{SNR}_{\text{optimal}}$  is quadratic in  $\text{SNR}_{ij}$ , so that  $\text{SNR}_{\text{optimal}}$  can be enhanced greatly if the individual  $\text{SNR}_{ij} \gg 1$ . The resulting optimal  $\text{SNR}_{\text{optimal}}$  for the four-detector correlation are shown in Table 6.

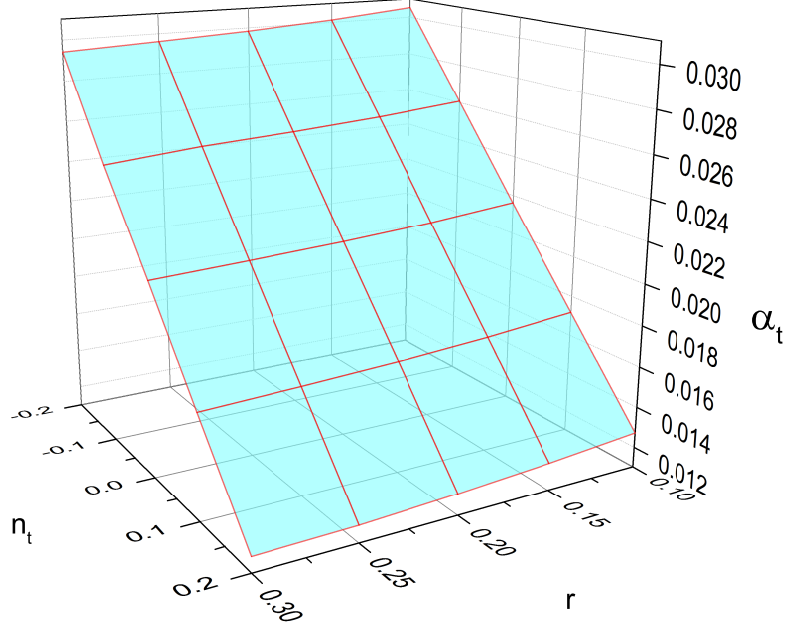


Figure 7: The upper limits of  $\alpha_t$  on the parameter plane  $(n_t, r)$ , allowed by the observational data of the pair of LIGO S6, to illustrate Table 3.

Table 5: The minimum  $\alpha_t$  required to detect by the multiple pairs from four detectors.

	$n_t = -0.1$	$n_t = 0$	$n_t = 0.1$
$r = 0.1$	0.02593	0.02149	0.01704
$r = 0.15$	0.02553	0.02109	0.01664
$r = 0.2$	0.02525	0.02080	0.01635
$r = 0.25$	0.02503	0.02058	0.01613
$r = 0.3$	0.02485	0.02040	0.01595

Similarly, requiring  $\text{SNR}_{\text{optimal}} > \text{SNR}_{\alpha, \gamma} = 3.30$ , yields the minimum  $\alpha_t$ , shown in Table 7.

Table 6:  $\text{SNR}_{\text{optimal}}$  of the four-detector correlation at  $r = 0.2$ .

$\alpha_t, n_t$	-0.005, -0.1	0, 0	0.005, 0.1	0.01, 0.2	0.015, 0.2
SNR	$4.8 \times 10^{-28}$	$1.0 \times 10^{-19}$	$2.1 \times 10^{-11}$	$4.8 \times 10^{-3}$	$1.3 \times 10^2$

Table 7: The minimum  $\alpha_t$  required to be detected by the four-detector correlation

	$n_t = -0.1$	$n_t = 0$	$n_t = 0.1$
$r = 0.1$	0.02714	0.02272	0.01830
$r = 0.15$	0.02675	0.02233	0.01791
$r = 0.2$	0.02647	0.02205	0.01763
$r = 0.25$	0.02625	0.02183	0.01741
$r = 0.3$	0.02607	0.02165	0.017123

## 5 Detection by six 2nd-generation detectors

The second-generation interferometers are currently under construction, their goal sensitivities will eventually reach  $10^{-24}$ , improving the sensitivity over the current detectors by more than an order. Correlating six 2nd-generation detectors will drastically increase SNRs and yield more stringent constraints on  $\alpha_t$ . We shall correlate six detectors: LIGO-Hanford(H), LIGO-Livingston(L), Virgo(V) [78], Kagra(K) [24], AIGO(A) [55], LIGO-India(I). LIGO-India will adopt the designed spectra of sensitivity of the advanced LIGO [56]. In our calculation, the BRSE mode for Kagra will be used since it has two operation modes. Also,  $T = 1.282$  years is assumed. From these six detectors one can construct fifteen correlated pairs. For each pair, Eq.(16) is used to calculate SNR. The calculated result is given in Table 8. Typically, for a pair of this kind of detectors,  $\text{SNR} \sim 10^{-6}$  for RGW of the default parameters, and the advanced LIGO H-L will enhance the capability by thousands of times than S6 in Table 1.

For six detectors there are also two ways of combination: multiple pairs and six-detector correlation [77].

### 5.1 multiple pairs

The squared optimal SNR of multiple pairs is [77]:

$$\begin{aligned}
 \text{SNR}_{\text{optimal}}^2 = & \text{SNR}_{\text{AH}}^2 + \text{SNR}_{\text{AI}}^2 + \text{SNR}_{\text{AK}}^2 + \text{SNR}_{\text{AL}}^2 + \text{SNR}_{\text{AV}}^2 \\
 & + \text{SNR}_{\text{HI}}^2 + \text{SNR}_{\text{HK}}^2 + \text{SNR}_{\text{HL}}^2 + \text{SNR}_{\text{HV}}^2 + \text{SNR}_{\text{IK}}^2 \\
 & + \text{SNR}_{\text{IL}}^2 + \text{SNR}_{\text{IV}}^2 + \text{SNR}_{\text{KL}}^2 + \text{SNR}_{\text{KV}}^2 + \text{SNR}_{\text{LV}}^2.
 \end{aligned} \tag{22}$$

The result is shown in Table 9, which are three orders greater than those of the multiple pairs of four detectors. The corresponding minimum  $\alpha_t$  is shown in Table 10, in particular, RGW can be directly detected by the six 2nd-generation detectors for models with  $\alpha_t > 0.01364$  for  $(n_t = 0, r = 0.2)$ . Similarly, the minimum  $n_t$  is calculated as  $n_t > 0.2982$  at  $r = 0.2$  and  $\alpha_t = 0$ . This is a much improved capability compared with that of LIGO H-L S6 and of the four 1st-generation detectors.

Table 8: SNR of fifteen pairs of 2nd generation detectors at  $r = 0.2$ .

$\alpha_t, n_t$	-0.005, -0.1	0, 0	0.005, 0.1	0.01, 0.2	0.015, 0.2
A-H	$2.3 \times 10^{-10}$	$2.0 \times 10^{-6}$	$1.9 \times 10^{-2}$	$1.7 \times 10^2$	$2.1 \times 10^4$
A-I	$1.9 \times 10^{-10}$	$1.6 \times 10^{-6}$	$1.4 \times 10^{-2}$	$1.2 \times 10^2$	$1.5 \times 10^4$
A-K	$3.8 \times 10^{-11}$	$3.5 \times 10^{-7}$	$3.5 \times 10^{-3}$	$3.5 \times 10^1$	$4.5 \times 10^3$
A-L	$2.4 \times 10^{-10}$	$2.1 \times 10^{-6}$	$1.9 \times 10^{-2}$	$1.8 \times 10^2$	$2.2 \times 10^4$
A-V	$4.4 \times 10^{-11}$	$4.3 \times 10^{-7}$	$4.4 \times 10^{-3}$	$4.5 \times 10^1$	$5.7 \times 10^3$
H-I	$1.1 \times 10^{-10}$	$9.7 \times 10^{-7}$	$9.1 \times 10^{-3}$	$8.8 \times 10^1$	$1.1 \times 10^4$
H-K	$2.2 \times 10^{-11}$	$2.1 \times 10^{-7}$	$2.1 \times 10^{-3}$	$2.1 \times 10^1$	$2.7 \times 10^3$
H-L	$6.7 \times 10^{-11}$	$6.1 \times 10^{-6}$	$5.7 \times 10^{-2}$	$5.4 \times 10^2$	$6.4 \times 10^4$
H-V	$5.5 \times 10^{-11}$	$5.5 \times 10^{-7}$	$5.5 \times 10^{-3}$	$5.7 \times 10^1$	$7.3 \times 10^3$
I-K	$5.4 \times 10^{-11}$	$5.1 \times 10^{-7}$	$5.0 \times 10^{-3}$	$5.1 \times 10^1$	$6.5 \times 10^3$
I-L	$1.9 \times 10^{-10}$	$1.7 \times 10^{-6}$	$1.6 \times 10^{-2}$	$1.5 \times 10^2$	$1.9 \times 10^4$
I-V	$3.6 \times 10^{-11}$	$3.4 \times 10^{-7}$	$3.4 \times 10^{-3}$	$3.4 \times 10^1$	$4.3 \times 10^3$
K-L	$6.9 \times 10^{-12}$	$6.6 \times 10^{-8}$	$6.5 \times 10^{-4}$	$6.5 \times 10^0$	$8.2 \times 10^2$
K-V	$3.8 \times 10^{-11}$	$4.0 \times 10^{-7}$	$4.2 \times 10^{-3}$	$4.5 \times 10^1$	$5.9 \times 10^3$
L-V	$5.8 \times 10^{-11}$	$5.8 \times 10^{-7}$	$5.9 \times 10^{-3}$	$6.2 \times 10^1$	$8.0 \times 10^3$

Table 9:  $\text{SNR}_{\text{optimal}}$  of the multiple pairs from six detectors at  $r = 0.2$ .

$\alpha_t, n_t$	-0.005, -0.1	0, 0	0.005, 0.1	0.01, 0.2	0.015, 0.2
optimal	$8.1 \times 10^{-10}$	$7.3 \times 10^{-6}$	$6.8 \times 10^{-2}$	$6.4 \times 10^2$	$7.8 \times 10^4$

## 5.2 six-detector correlation

Similarly, the squared optimal SNR for six-detector correlation is [77]:

$$\begin{aligned}
 \text{SNR}_{\text{optimal}}^2 = & \text{SNR}_{\text{AH}}^2 \text{SNR}_{\text{IK}}^2 \text{SNR}_{\text{LV}}^2 + \text{SNR}_{\text{AH}}^2 \text{SNR}_{\text{IL}}^2 \text{SNR}_{\text{KV}}^2 \\
 & + \text{SNR}_{\text{AH}}^2 \text{SNR}_{\text{IV}}^2 \text{SNR}_{\text{KL}}^2 + \text{SNR}_{\text{AI}}^2 \text{SNR}_{\text{HK}}^2 \text{SNR}_{\text{LV}}^2 \\
 & + \text{SNR}_{\text{AI}}^2 \text{SNR}_{\text{HV}}^2 \text{SNR}_{\text{KL}}^2 + \text{SNR}_{\text{AI}}^2 \text{SNR}_{\text{HV}}^2 \text{SNR}_{\text{KL}}^2 \\
 & + \text{SNR}_{\text{AK}}^2 \text{SNR}_{\text{HI}}^2 \text{SNR}_{\text{LV}}^2 + \text{SNR}_{\text{AK}}^2 \text{SNR}_{\text{HL}}^2 \text{SNR}_{\text{IV}}^2 \\
 & + \text{SNR}_{\text{AK}}^2 \text{SNR}_{\text{HV}}^2 \text{SNR}_{\text{IL}}^2 + \text{SNR}_{\text{AL}}^2 \text{SNR}_{\text{HI}}^2 \text{SNR}_{\text{KV}}^2 \\
 & + \text{SNR}_{\text{AL}}^2 \text{SNR}_{\text{HK}}^2 \text{SNR}_{\text{IV}}^2 + \text{SNR}_{\text{AL}}^2 \text{SNR}_{\text{HV}}^2 \text{SNR}_{\text{IK}}^2 \\
 & + \text{SNR}_{\text{AV}}^2 \text{SNR}_{\text{HI}}^2 \text{SNR}_{\text{LK}}^2 + \text{SNR}_{\text{AV}}^2 \text{SNR}_{\text{HK}}^2 \text{SNR}_{\text{IL}}^2 \\
 & + \text{SNR}_{\text{AV}}^2 \text{SNR}_{\text{HV}}^2 \text{SNR}_{\text{IK}}^2,
 \end{aligned} \tag{23}$$

The calculated result is shown in Table 11. One notices that, in this case, the optimal  $\text{SNR}_{\text{optimal}}$  is cubic in  $\text{SNR}_{ij}$ , and its dependence on  $(n_t, \alpha_t)$  is different from that of the multiple method. For instance, for the default  $(n_t = 0, \alpha_t = 0)$ ,  $\text{SNR}_{\text{optimal}}$  of six-detector correlation is smaller than  $\text{SNR}_{\text{optimal}}$  of multiple-pairs. However, for greater values of  $(n_t, \alpha_t)$ ,  $\text{SNR}_{\text{optimal}}$  of six-detector correlation trends to be much greater than  $\text{SNR}_{\text{optimal}}$  of multiple-pairs. The minimum  $\alpha_t$  for detection are in Table 12.

Table 10: The minimum  $\alpha_t$  required to be detected by the multiple pairs from six detectors.

$n_t = -0.2$	$n_t = -0.1$	$n_t = 0$	$n_t = 0.1$
$r = 0.1$	0.01893	0.01437	0.00979
$r = 0.15$	0.01851	0.01394	0.00937
$r = 0.2$	0.01821	0.01364	0.00907
$r = 0.25$	0.01798	0.01341	0.00884
$r = 0.3$	0.01779	0.01322	0.00865

Table 11:  $\text{SNR}_{\text{optimal}}$  of the six-detector correlation, at  $r = 0.2$ .

$\alpha_t, n_t$	-0.005, -0.1	0, 0	0.005, 0.1	0.01, 0.2	0.015, 0.2
6 detectors	$5.6 \times 10^{-30}$	$4.5 \times 10^{-18}$	$7.0 \times 10^{-6}$	$3.7 \times 10^6$	$3.2 \times 10^{12}$

### 5.3 How many detectors do we need?

Here comes a question: how many interferometers do we need to detect the RGW? To a large extent, this depends on the parameters of RGW. As an example, we can give an estimate for the multiple pairs method. According to Eq.(5.46) in Ref.[77], for  $N$  detectors of the same level sensitivity, one has

$$\text{SNR}_{\text{optimal}}^2 = \sum_{i < j}^N \text{SNR}_{ij}^2 \simeq \frac{N(N-1)}{2} \text{SNR}_{ij}^2. \quad (24)$$

By  $\text{SNR}_{ij} \sim 10^{-6}$  for the default parameters based on the second-generation detectors,

$$\text{SNR}_{\text{optimal}} \simeq 10^{-6} \sqrt{\frac{N(N-1)}{2}}. \quad (25)$$

Then  $N \simeq 10^6$  detectors would be required for  $\text{SNR}_{\text{optimal}}$  to be greater than 1. Nevertheless, the chance to detect RGW is largely dependent on  $n_t$  and  $\alpha_t$ . For slightly greater values, say  $\alpha_t = 0.02$  and  $n_t = 0$  within the constraint of Eq.(19), six detectors will be enough to detect RGW at a high significance with  $\text{SNR} \simeq 10^3$ .

## 6 Conclusion

Based on the analytical solution of RGW, covering the whole five stages of cosmic expansion, the resulting spectrum of RGW contains the three parameters  $(n_t, \alpha_t, r)$ , that are determined by the initial condition during the inflation. We take the amplitude of the spectrum so that its low frequency end is equal to that of the primordial spectrum, leading to a modification by  $\sim 1/50$  to the previous result.

We have constrained  $(n_t, \alpha_t, r)$  of the analytical spectrum, using the interferometer detectors. The SNR of RGW are calculated for various values of  $(n_t, \alpha_t, r)$ , based on the sensitivity data of S6 of LIGO HL pair. The amplitude of RGW is very sensitive to  $\alpha_t$  at high frequencies  $10^2 - 10^3 \text{Hz}$ . We have derived the upper limits  $\alpha_t \leq 0.02093$  at  $r = 0.2$  and  $n_t = 0$ , and  $n_t < 0.470$  at  $(\alpha_t = 0, r = 0.2)$ . This is the first constraint upon  $\alpha_t$  based on actual observations, also consistent with the constraint on the energy density



Table 12: The minimum  $\alpha_t$  by 6-detector correlation.

$n_t = -0.2$	$n_t = -0.1$	$n_t = 0$	$n_t = 0.1$
$r = 0.1$	0.01958	0.014302	0.01046
$r = 0.15$	0.01916	0.01460	0.01004
$r = 0.2$	0.01886	0.01430	0.00974
$r = 0.25$	0.01863	0.01407	0.00951
$r = 0.3$	0.01844	0.01388	0.00932

obtained by LIGO-Virgo Collaboration. CMB observations so far have little constraint on the indices  $n_t$  and  $\alpha_t$ . Thus, in regard to detections of RGW, the interferometers method and the CMB observations are complementary, working at different frequencies.

We have also explored the detection of RGW by four 1st generation, and six 2nd generation detectors, in two different optimal combinations. We have calculated SNR in each case, and found that the chance to detect RGW is largely dependent on  $n_t$  and  $\alpha_t$  of RGW itself. RGW can be directly detected by the six 2nd-generation detectors for models with  $\alpha_t > 0.01364$  at  $r = 0.2$  and  $n_t = 0$ , or  $n_t > 0.2982$  at  $r = 0.2$  and  $\alpha_t = 0$ .

We thank Dr. Nishizawa for helpful information and discussions. Y. Zhang is supported by NSFC Grant No. 11275187, NSFC 11421303, SRFDP, and CAS, the Strategic Priority Research Program "The Emergence of Cosmological Structures" of the Chinese Academy of Sciences, Grant No. XDB09000000.

## References

- [1] L. P. Grishchuk, *Amplification of gravitational waves in an isotropic universe*, *Sov. Phys. JETP* **40**(1975) 409.
- [2] L. P. Grishchuk, *Quantum Effects In Cosmology*, *Class. Quant. Grav.* **10** (1993) 2449 [gr-qc/9302036].
- [3] L. P. Grishchuk, *The Implications of the Microwave Background Anisotropies for Laser-Interferometer-Tested Gravitational Waves*, *Class. Quant. Grav.* **14** (1997) 1445 [gr-qc/9609062].
- [4] L. P. Grishchuk, *Relic Gravitational Waves and Their Detection*, *Lecture Notes in Physics*, Vol.**562** (2001) 167, Springer-Verlag [gr-qc/0002035].
- [5] A. A. Starobinsky, *Cosmic Background Anisotropy Induced by Isotropic Flat-Spectrum Gravitational-Wave Perturbations*, *Sov. Astron. Lett.* **11** (1985) 133.
- [6] V. A. Rubakov, M. V. Sazhin and A. V. Veryaskin, *Graviton creation in the inflationary universe and the grand unification scale*, *Phys. Lett. B.* **115** (1982) 189
- [7] R. Fabbri and M.D. Pollock, *The effect of primordially produced gravitons upon the anisotropy of the cosmological microwave background radiation*, *Phys. Lett. B.* **125** (1983) 445.
- [8] L.F. Abbott and M.B. Wise, *Constraints on generalized inflationary cosmologies*, *Nucl. Phys. B.* **244** (1984) 541.

- [9] B. Allen, *Stochastic gravity-wave background in inflationary-universe models*, *Phys. Rev. D* **37** (1988) 2078.
- [10] B. Allen and S. Koranda, *CBR anisotropy from primordial gravitational waves in inflationary cosmologies*, *Phys. Rev. D* **50** (1994) 3713 [astro-ph/9404068].
- [11] V. Sahni, *Energy density of relic gravity waves from inflation*, *Phys. Rev. D.* **42** (1990) 453.
- [12] H. Tashiro, T. Chiba and M. Sasaki, *Reheating After Quintessential Inflation and Gravitational Waves*, *Class. Quantum Grav.* **21** (2004) 1761 [gr-qc/0307068].
- [13] A. B. Henriques, *The stochastic gravitational-wave background and the inflation to radiation transition in the early universe*, *Class. Quantum Grav.* **21** (2004) 3057.
- [14] P. M. Sá and A. B. Henriques, *Gravitational wave generation in hybrid quintessential inflationary models*, *Phys. Rev. D.* **81** (2010) 124043 [arXiv:1003.4112].
- [15] M. Giovannini, *Production and detection of relic gravitons in quintessential inflationary models*, *Phys. Rev. D.* **60** (1999) 123511 [astro-ph/9903004].
- [16] M. Giovannini, *Spikes in the Relic Graviton Background from Quintessential Inflation*, *Class. Quant. Grav.* **16** (1999) 2905 [hep-ph/9903263].
- [17] M. Maggiore, *Gravitational Wave Experiments and Early Universe Cosmology*, *Phys. Rept.* **331** (2000) 283 [gr-qc/9909001].
- [18] W. Zhao and Y. Zhang, *Relic gravitational waves and their detection*, *Phys. Rev. D.* **74** (2006) 043503 .
- [19] <http://www.ligo.caltech.edu>
- [20] <http://virgo.infn.it/>
- [21] A. Freise *et al.*, *Status of VIRGO*, *Class. Quantum Grav.* **22** (2005) S869 [gr-qc/0406123].
- [22] <http://www.geo600.org/>
- [23] B. Willke *et al.* *The GEO 600 gravitational wave detector*, *Class. Quantum Grav.* **19** (2002) 1377;
- [24] <http://gwcenter.icrr.u-tokyo.ac.jp/en/>
- [25] K. Kuroda, *Status of LCGT*, *Class Quantum Grav.* **27** (2010) 084004.
- [26] K. Somiya, *Detector configuration of KAGRA - the Japanese cryogenic gravitational-wave detector*, *Class. Quantum Grav.* **29** (2012) 124007 [arXiv:1111.7185].
- [27] <http://lisa.nasa.gov/>.
- [28] <http://elisa-ngo.org/>.
- [29] P. Amaro-Seoane *et al.*, *Low-frequency gravitational-wave science with eLISA/NGO*, *Class. Quantum Grav.* **29** (2012) 124016 [arXiv:1202.0839].

- [30] G. Hobbs, *Pulsars and Gravitational Wave Detection*, *PASA*, **22**(2005) 179 [astro-ph/0412153].
- [31] G.Hobbs, *Gravitational wave detection using high precision pulsar observations*, *Class. Quantum Grav.*, **25** (2008) 114032 [arXiv:0802.1309].
- [32] <http://www.ipta4gw.org/>
- [33] <http://www.skatelescope.org/>
- [34] <http://fast.bao.ac.cn/en/>
- [35] <http://map.gsfc.nasa.gov/>
- [36] C. L. Bennett *et al.*, *First Year Wilkinson Microwave Anisotropy Probe (WMAP) Observations: Preliminary Maps and Basic Results* , *ApJS* **148** (2003) 1 [arXiv:astro-ph/0302207].
- [37] E. Komatsu, *et al.*, *Seven-year Wilkinson Microwave Anisotropy Probe (WMAP) Observations: Cosmological Interaction*, *Astrophys. J. Suppl.* **192** (2011) 18 [arXiv:1001.4538].
- [38] G. Hinshaw *et al.*, *Nine-Year Wilkinson Microwave Anisotropy Probe (WMAP) Observations: Cosmological Parameter Results*, [arXiv:1212.5226].
- [39] C. L. Bennett, *et al.*, *Nine-Year Wilkinson Microwave Anisotropy Probe (WMAP) Observations: Final Maps and Results*, [arXiv:1212.5225].
- [40] <http://www.cosmos.esa.int/web/planck>
- [41] Planck Collaboration, *Planck 2013 results. XXII. Constraints on inflation* , *Astron. Astrophys.* **571** (2014) A22 [arXiv:1303.5082v3].
- [42] <https://www.cfa.harvard.edu/CMB/bicep2/>
- [43] BICEP2 collaboration, *BICEP2 I: Detection of B-mode Polarization at Degree Angular Scales*, *Phys. Rev. Lett.* **112** (2014) 241101 [arXiv:1403.3985].
- [44] J. Aasi *et al.*, *Improved Upper Limits on the Stochastic Gravitational-Wave Background from 2009-2010 LIGO and Virgo Data*, *Phys. Rev. Lett.* **113** (2014) 231101 [arXiv:1406.4556v2].
- [45] Planck Collaboration, *Planck intermediate results. XXX. The angular power spectrum of polarized dust emission at intermediate and high Galactic latitudes*, [arXiv:1409.5738v1].
- [46] Y. Zhang, Y.F. Yuan, W. Zhao and Y.T. Chen, *Relic gravitational waves in the accelerating Universe*, *Class. Quantum Grav.* **22** (2005) 1383.
- [47] Y. Zhang, X. Z. Er, T. Y. Xia, W. Zhao and H. X. Miao, *An exact analytic spectrum of relic gravitational waves in an accelerating universe*, *Class. Quantum Grav.* **23** (2006) 3783.
- [48] H. X. Miao and Y. Zhang, *Analytic spectrum of relic gravitational waves modified by neutrino free streaming and dark energy*, *Phys. Rev. D* **75** (2007) 104009.

- [49] S. Wang, Y. Zhang, T. Y. Xia, and H. X. Miao, *Modifications by QCD transition and  $e^+e^-$  annihilation on analytic spectrum of relic gravitational waves in accelerating universe*, *Phys. Rev D* **77** (2008) 104016 [arXiv:0803.2707].
- [50] M.L. Tong and Y. Zhang, *Relic Gravitational Waves with A Running Spectral Index and Its Constraints at High Frequencies*, *Phys. Rev. D* **80** (2009) 084022 [arXiv:0910.0325].
- [51] Y. Zhang, M.L. Tong, and Z.W. Fu, *Constraints upon the spectral indices of relic gravitational waves by LIGO S5*, *Phys. Rev. D* **81** (2010) 101501(R) [arXiv:1004.2944].
- [52] The LIGO Collaboration and The Virgo Collaboration, *An upper limit on the stochastic gravitational-wave background of cosmological origin*, *Nature* **460** (2009) 990.
- [53] J. Abadie *et al.*, *Sensitivity Achieved by the LIGO and Virgo Gravitational Wave Detectors during LIGO's Sixth and Virgo's Second and Third Science Runs*, arXiv:1203.2674v2.
- [54] G. M. Harry (for LIGO Scientific Collaboration), *Advanced LIGO: the next generation of gravitational wave detectors*, *Class. Quantum Grav.* **27** (2010) 084006 .
- [55] P. Barriga *et. al*, *AIGO: a southern hemisphere detector for the worldwide array of ground-based interferometric gravitational wave detectors*, *Class. Quantum Grav.* **27** (2010) 084005.
- [56] B. Iyer, *et.al*, *LIGO-India, Proposal of the Consortium for Indian Initiative in Gravitational-wave Observations (IndIGO)*, <https://dcc.ligo.org/cgi-bin/DocDB/ShowDocument?docid=75988>
- [57] S. Fairhurst, *Improved source localization with LIGO India*, *J. Phys.: Conf. Ser.* **484** (2014) 012007 [arXiv:1205.6611v2].
- [58] L. Parker, *The production of elementary particles by strong gravitational fields* *Asymptotic Structure of Space-Time*, ed S. Deser and M. Levy (New York: Plenum) (1979).
- [59] L. P. Grishchuk, *Signatures of Quantum Gravity in the Large-Scale Universe*, [arXiv:gr-qc/9708070].
- [60] M.L Tong *et al.*, *Using pulsar timing arrays and the quantum normalization condition to constrain relic gravitational waves*, *Class. Quantum Grav.* **31** (2014) 035001 [arXiv:1311.7192].
- [61] A. Kosowsky, M.D. Turner, *CBR anisotropy and the running of the scalar spectral index*, *Phys. Rev. D* **52** (1995) 1739.
- [62] A.R. Liddle and D.H. Lyth, *The Cold Dark Matter Density Perturbation*, *Phys. Rep.* **231** (1993) 1 [ arXiv:astro-ph/9303019].
- [63] J. Garcia-Bellido and D. Wands, *The spectrum of curvature perturbations from hybrid inflation*, *Phys.Rev. D* **53** (1996) 5437 [arXiv:astro-ph/9606047].
- [64] J. Garriga, V.F. Mukhanov, *Perturbations in k-inflation*, *Phys. Lett. B* **458** (1999) 219 [arXiv:hep-th/9904176].

- [65] N. Bartolo, S. Matarrese, A. Riotto, *Adiabatic and Isocurvature Perturbations from Inflation: Power Spectra and Consistency Relation*, *Phys.Rev. D* **64** (2001) 123504 [arXiv:astro-ph/0107502].
- [66] S. Tsujikawa, D. Parkinson, and B. A. Bassett, *Aspects of String-Gas Cosmology at Finite Temperature*, *Phys.Rev. D* **67** (2003) 083516 [arXiv:hep-th/0301180].
- [67] S. Das, S. Mukherjee, and T. Souradeep, *Revised cosmological parameters after BICEP 2 and BOSS*, *JCAP* **02** (2015) 016 [arXiv:1406.0857].
- [68] W.Zhao and Y.Zhang, *Analytic approach to the CMB polarizations generated by relic gravitational waves*, *Phys. Rev. D* **74** (2006) 083006 [arXiv:astro-ph/0508345].
- [69] T.Y. Xia and Y. Zhang, *Analytic spectra of CMB anisotropies and polarization generated by relic gravitational waves with modification due to neutrino free-streaming*, *Phys.Rev. D* **78** (2008) 123005.
- [70] T.Y. Xia and Y. Zhang, *Approximate analytic spectra of reionized CMB anisotropies and polarization generated by relic gravitational waves*, *Phys.Rev. D* **79** (2009) 083002.
- [71] Z. Cai and Y.Zhang, *Analytic Spectra of CMB Anisotropies and Polarization Generated by Scalar Perturbations in Synchronous Gauge*, *Class. Quantum Grav.* **29** (2012) 105009 [arXiv:1204.6683].
- [72] M. L. Tong, Y. Zhang, and F. Y. Li, *Using polarized maser to detect high-frequency relic gravitational waves*, *Phys.Rev. D* **78** (2008) 024041 [arXiv:0807.0885].
- [73] L. Parker, *Amplitude of Perturbations from Inflation* [arXiv:hep-th/0702216].
- [74] I. Agullo, J. Navarro-Salas, G. J. Olmo and L. Parker, *The Power Spectrum in de Sitter Inflation, Revisited*, *Phys. Rev. Lett.* **101** (2008) 171301 [arXiv:0806.0034].
- [75] I. Agullo, J. Navarro-Salas, G. J. Olmo and L. Parker, *Revising the observable consequences of slow-roll inflation*, *Revising the observable consequences of slow-roll inflation*, *Phys. Rev. D* **81** (2010) 043514.
- [76] E. Flanagan, *The Sensitivity of Ligo to a Stochastic Background, and its Dependence on the Detector Orientations*, *Phys.Rev.D* **48** (1993) 2389 [arXiv:astro-ph/9305029].
- [77] B. Allen and J.D. Romano, *Detecting a stochastic background of gravitational radiation: Signal processing strategies and sensitivities*, *Phys. Rev. D* **59** (1999) 102001 [arXiv:gr-qc/9710117].
- [78] The LIGO Collaboration and The Virgo Collaboration, *Prospects for Localization of Gravitational Wave Transients by the Advanced LIGO and Advanced Virgo Observatories*, arXiv:1304.0670
- [79] A.Nishizawa *et al.*, *Probing non-tensorial polarizations of stochastic gravitational-wave backgrounds with ground-based laser interferometers*, *Phys. Rev. D* **79** (2009) 082002 [arXiv:0903.0528].
- [80] N. Seto and A. Taruya, *Polarization analysis of gravitational-wave backgrounds from the correlation signals of ground-based interferometers: measuring a circular-polarization mode*, *Phys. Rev. D* **77** (2008) 103001 [arXiv:0801.4185].

# Appendix

In the expression of SNR in Eq.(16), the overlapping function  $\gamma(f)$  between a pair of two detectors  $i$  and  $j$  appears. To calculate  $\gamma(f)$ , one needs to know the positions and directions of the two detectors in the pair. The overlapping function between the detectors  $i$  and  $j$  is defined by [76, 77, 79]:

$$\gamma(f) = \Theta_+(\alpha, \beta) \cos(4\sigma_+) + \Theta_-(\alpha, \beta) \cos(4\sigma_-), \quad (26)$$

where

$$\begin{aligned} \Theta_+(\alpha, \beta) &\equiv -\left(\frac{3}{8}j_0 - \frac{45}{56}j_2 + \frac{169}{896}j_4\right) + \left(\frac{1}{2}j_0 - \frac{5}{7}j_2 - \frac{27}{224}j_4\right) \cos \beta \\ &\quad - \left(\frac{1}{8}j_0 + \frac{5}{56}j_2 + \frac{3}{896}j_4\right) \cos 2\beta, \\ \Theta_-(\alpha, \beta) &\equiv \left(j_0 + \frac{5}{7}j_2 + \frac{3}{112}j_4\right) \cos\left(\frac{\beta}{2}\right)^4, \end{aligned}$$

consisting of  $j_n = j_n(\alpha)$  is the spherical Bessel's functions. In the above,  $\beta$  is the angle formed by the two detectors measured at the center of the Earth,  $\alpha$  is the phase difference between the two detectors due to the separation  $|\Delta\vec{X}|$  of the two detectors:

$$\alpha(f) = 2\pi f \frac{|\Delta\vec{X}|}{c}, \quad |\Delta\vec{X}| = |\vec{X}_i - \vec{X}_j| = 2R_E \sin \frac{\beta}{2},$$

with  $R_E = 6371\text{km}$  being the radius of Earth. In Eq.(26),

$$\sigma_+ = \frac{1}{2}(\sigma_i + \sigma_j), \quad \sigma_- = \frac{1}{2}(\sigma_i - \sigma_j),$$

where  $\sigma_i$  is the angle between the tangent line of the great circle connecting the two detectors and the bisector between two arms of the detector  $i$ , and  $\sigma_j$  is for  $j$ , schematically shown in Fig 8.

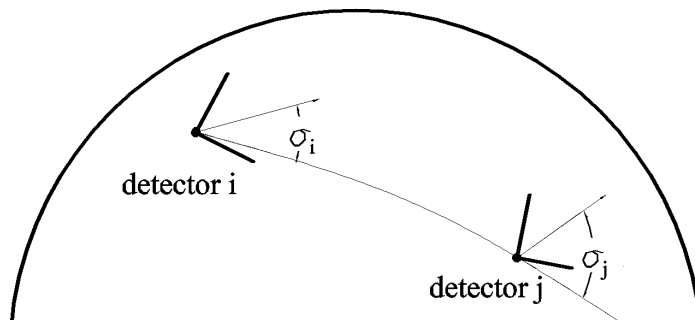


Figure 8: The angles  $\sigma_i$  and  $\sigma_j$  are schematically shown for two detectors  $i$  and  $j$  on the Earth.

In this paper, seven detectors are considered, AIGO(A), Geo(G), LIGO-Hanford(H), LIGO-India(I), Kagra(K), LIGO-Livingston(L), and Virgo(V). Information of the positions and directions of seven detectors is listed in Table 13 [79], [80], [56]. The position

of a detector on the Earth is fixed by  $\theta$  and  $\phi$  in the spherical coordinate.  $\psi$  is the angle between the local east direction and the bisecting line of two arms measured counterclockwise. From these given values, we have calculated  $(\beta, \sigma_+, \sigma_-)$  of the relevant pairs, and the result is given in Tab.14. In Ref. [79], some of the values of  $\sigma_+$  and  $\sigma_-$  are different from ours in Table 14. Ref. [79] has adjusted the values of  $\sigma_+$  and  $\sigma_-$  by an integer times of  $90^\circ$ . This brings no difference to  $\cos(4\sigma_+)$  and  $\cos(4\sigma_-)$  that appear in the overlapping function  $\gamma(f)$ .

Table 13: Positions and orientations of seven interferometers on the Earth (in units of degree)

detector	$\theta$	$\phi$	$\psi$
<i>A</i>	121.4	115.7	-45.0
<i>G</i>	47.7	9.8	68.8
<i>H</i>	43.5	-119.4	171.8
<i>I</i>	70.9	74.05	135.0
<i>K</i>	35.6	137.3	70.0
<i>L</i>	59.4	-90.8	243.0
<i>V</i>	46.4	10.5	116.5

Table 14: Angles and separations appearing in  $\gamma(f)$  for the relevant pairs

detector pair	$\beta$ ( $^\circ$ )	$ \Delta\vec{X} (km)$	$\sigma_+$ ( $^\circ$ )	$\sigma_-$ ( $^\circ$ )
<i>A - H</i>	135.6	$1.18 \times 10^4$	-44.9	-36.3
<i>A - I</i>	64.4	$6.79 \times 10^3$	3.4	-182.6
<i>A - K</i>	70.8	$7.38 \times 10^3$	-148.6	31.9
<i>A - L</i>	157.3	$1.25 \times 10^4$	2.1	-52.0
<i>A - V</i>	121.4	$1.11 \times 10^4$	-29.2	-160.8
<i>G - H</i>	80.4	$8.23 \times 10^3$	31.7	-85.6
<i>G - L</i>	77.0	$7.93 \times 10^3$	60.0	-141.4
<i>G - V</i>	1.4	$1.55 \times 10^2$	-65.8	65.9
<i>H - I</i>	113.3	$1.06 \times 10^4$	61.5	6.5
<i>H - K</i>	72.4	$7.52 \times 10^3$	25.6	0.9
<i>H - L</i>	27.2	$3.00 \times 10^3$	152.2	45.3
<i>H - V</i>	79.6	$8.16 \times 10^3$	55.1	66.1
<i>I - K</i>	57.5	$6.13 \times 10^3$	-2.9	106.3
<i>I - L</i>	128.2	$1.15 \times 10^4$	99.8	-71.5
<i>I - V</i>	58.0	$6.18 \times 10^3$	57.6	-62.5
<i>K - L</i>	99.2	$9.71 \times 10^3$	68.1	-47.6
<i>K - V</i>	86.6	$8.74 \times 10^3$	5.6	-61.1
<i>L - V</i>	76.8	$7.91 \times 10^3$	83.1	116.7